PAPER NAME

LnPO4:Eu3+ nanoparticles: role of host l attices on physiochemical and luminesce nt properties

AUTHOR

-

WORD COUNT

6564 Words

CHARACTER COUNT

36430 Characters

PAGE COUNT

24 Pages

FILE SIZE

1.4MB

SUBMISSION DATE

Sep 16, 2023 9:04 AM GMT+3

REPORT DATE

Sep 16, 2023 9:04 AM GMT+3

24% Overall Similarity

The combined total of all matches, including overlapping sources, for each database.

- 12% Internet database
- Crossref database
- 0% Submitted Works database
- 23% Publications database
- Crossref Posted Content database

Excluded from Similarity Report

- Bibliographic material

Journal of King Saud University - Science

LnPO4:Eu3+ nanoparticles: role of host lattices on physiochemical and luminescent properties

--Manuscript Draft--

Manuscript Number:	
Article Type:	Full length article
Section/Category:	Chemistry
Keywords:	Metal phosphates; europium; crystallographic; optical bandgap; luminescent
Abstract:	LnPO4:Eu3+ (Ln=La, Gd and Y) nanoparticles (NPs) were prepared at low temperatures via a urea-based thermal decomposition method. A systematic comparative characteristic was presented to explore the impact of the host lattices on crystal structure, crystallinity, surface behavior, colloidal dispersibility, Raman shift, bandgap energy, and luminescent properties. X-ray diffraction pattern revealed a hexagonal single phase, high purity with an average crystalline size of 13.9, 14.89, and 18.7 nm for LaPO4:Eu, GdPO4:Eu, and YPO4:Eu NPs, respectively. Lattice parameters were also calculated to examine the effect of the crystallinity and crystal symmetry. FTIR spectra exhibited a broad IR band at higher frequency causing the surface to attach physically adsorbed water molecules. Metal phosphate is easily dispersible in aqueous media as represented by the UV/Visible absorption spectra. Raman shift was also recorded to examine the active vibrational modes of the metal phosphates. Bandgap energies were calculated based on the measure absorption spectra are to be values 5.14, 5.03, and 4.90 eV for the LaPO4:Eu, GdPO4:Eu, and YPO4:Eu NPs, respectively. A comparative study suggested that the excitation and emission transitions were significantly higher in the GdPO4:Eu NPs and in comparison to the LaPO4:Eu and YPO4:Eu NPs. Although, the sensitivity of the photoluminescent transitions was in the order GdPO4:Eu>YPO4:Eu>LaPO4:Eu NPs. Magnetic-dipole 5D0→7F1 emission line was foremost compared to the electric dipole 5D0→7F2 transition in the LaPO4:Eu NPs, whereas, electric-dipole 5D0→7F2 transition was dominant in the GdPO4:Eu and YPO4:Eu NPs over the magnetic-dipole 5D0→7F1 transition. It implies the impact of the crystallinity, host lattice, and crystal symmetry, in which doped Eu3+-ion replaces the host cation and distorts the crystal symmetry.

$LnPO_4:Eu^{3+}$ nanoparticles: role of host lattices on physiochemical and luminescent properties

Abstract

$LnPO_4:Eu^{3+}$ (Ln=La, Gd and Y) nanoparticles (NPs) were prepared at low temperatures via a urea-based thermal decomposition method. A systematic comparative characteristic was presented to explore the impact of the host lattices on crystal structure, crystallinity, surface behavior, colloidal dispersibility, Raman shift, bandgap energy, and luminescent properties. X-ray diffraction pattern revealed a hexagonal single phase, high purity with an average crystalline size of 13.9, 14.89, and 18.7 nm for $LaPO_4$:Eu, $GdPO_4$:Eu, and YPO_4:Eu NPs, respectively. Lattice parameters were also calculated to examine the effect of the crystallinity and crystal symmetry. FTIR spectra exhibited a broad IR band at higher frequency causing the surface to attach physically adsorbed water molecules. Metal phosphate is easily dispersible in aqueous media as represented by the UV/Visible absorption spectra. Raman shift was also recorded to examine the active vibrational modes of the metal phosphates. Bandgap energies were calculated based on the measure absorption spectra are to be values 5.14, 5.03, and 4.90 eV for the $LaPO_4$:Eu, $GdPO_4$:Eu, and YPO_4:Eu NPs, respectively. A comparative study suggested that the excitation and emission transitions were significantly higher in the $GdPO_4$:Eu NPs and in comparison to the $LaPO_4$:Eu and YPO_4:Eu NPs. Although, the sensitivity of the photoluminescent transitions was in the order $GdPO_4$:Eu>YPO_4:Eu>$LaPO_4$:Eu NPs. Magnetic-dipole $^5D_0 \rightarrow {}^7F_1$ emission line was foremost compared to the electric dipole $^5D_0 \rightarrow {}^7F_2$ transition in the $LaPO_4$:Eu NPs, whereas, electric-dipole $^5D_0 \rightarrow {}^7F_2$ transition was dominant in the $GdPO_4$:Eu and YPO_4:Eu NPs over the magnetic-dipole $^5D_0 \rightarrow {}^7F_1$ transition. It implies the impact of the crystallinity, host lattice, and crystal symmetry, in which doped Eu^{3+}-ion replaces the host cation and distorts the crystal symmetry.

Keywords: Metal phosphates, europium, crystallographic, optical bandgap, luminescent

1. Introduction

Currently, luminescent materials are a subject of much interest to researchers because of their usage in a broad range of applications in applied material and biomedical sciences [1-3]. Luminescent materials are used in the development of laser diodes, which are further used in hospitals as a surgical tool, which is a non-invasive technique. Similarly, luminescent materials in penal displays, lasers, photocatalysis, thermometry, optical biosensors, and many more applications [1, 4, 5]. Till now, a large number of organic dyes, semiconductor materials, and plasmonic nanomaterials have been applied as luminescent materials. But because of their weak chemical photo-stability, thermally unstable, photo-bleaching, autofluorescence, short decay time, low biocompatibility, and toxic nature reduced their applicability in clinical trials and other photonic-based applications[6, 7]. In comparison to them, luminescent lanthanide (Ln^{3+}) materials reported unique optical properties including, sharp absorption & emission transition in a wide spectral range(ultraviolet-Visible-Infrared region), free of autofluorescence, long decay time, high thermal, photochemical stability, anti-Stock shift, biocompatible and less toxic[8, 9]. These unique characteristics draw the attention of physicists, chemists, and biologists for their future use as per current applications [3, 10].

Among the investigated host matrixes oxide-derived nanomaterials were exploited as an important host lattice for the doping of the luminescent Ln^{3+}-ions. Because oxide derived nanomaterials display superior physiochemical properties which differ from their respective metal fluoride host nanomaterials. In particular, metal orthophosphate is a much more explored category of the oxide-derived host matrices, because of their superior thermal (~2300^{o}C), weak solubility, photo-chemical robustness, resistance to photo-bleaching, and minimized phonon energy. Because of their strong thermo-chemical stability and high refractive index, $LnPO_4$ was utilized in a variety of applications, such as thermometry, laser diodes, humidity sensors, nuclear surplus removal agents, catalysts, biological probes, and medical analytical materials. The metal orthophosphates are an excellent host for doping of the other activator Ln^{3+} ions due to their high visual opacity and phonon energy up to 1100 cm^{-1}. These luminescent metal phosphates are valued for their high energy conversion rates, spectrum color purity, and high thermos-chemical stabilities. Various polymorphism forms of Ln^{3+} orthophosphates exist, including churchite or weinschenkite (monoclinic; naturally frequent), rhabdophane

(hexagonal), zircon or xenotime (tetragonal), monazite or monazite (monoclinic), and orthorhombic. These forms rely on the cation radii, crystallization circumstances, and preparation processes. It is current market demand to develop single laser-based materials with high sensitivity, and photo-stability, which can be utilized in particular technology-based applications. So that various synthesis methods have been developed for the synthesis of the $LnPO_4$ NPs and their applications.

Up to now, various synthesis processes were described by various researchers for the successful preparation of the $LnPO_4$ NPs[11-13]. Among them, the majority of the developed techniques for the preparation of $LnPO_4$ NPs rely on the co-precipitation process. One of the most popular techniques for the synthesis of $LnPO_4$ NPs is co-precipitation [14, 15]. The foundation of this procedure is a chemical exchange relationship that precipitates an insoluble inorganic molecule[16]. The simplicity and low cost of this technology are its main benefits. To create nanocrystals with minimized aggregation, tiny particle diameter, and monodispersed certain conditions must be met[17]. Additionally, the water-containing reaction environment might cause a substantial amount of water to be soaked on the exterior of the nanocrystal[18, 19]. Lai et al. applied a hydrothermal method for the preparation of hexagonal $LaPO_4$:Eu NPs[13]. Zhang et al used a urea-assisted well-dispersed co-precipitation procedure for the synthesis of uniform YPO_4:Eu hollow spheres[20, 21].

Here, we presented the physiochemical and photoluminescent properties of the optically active $LaPO_4$:Eu, $GdPO_4$:Eu and YPO_4:Eu NPs prepared at low-temperature under a urea-based thermal decomposition process. We constant all the synthesis parameters including doping of the activator ion, temperature, solution medium, powder calcination temperature, etc to control the physiochemical characteristics of all three samples. Systematic properties are presented to examine the influence of the host lattice, crystallinity, surface behavior, Raman shift, optical activity, colloidal stability, and photoluminescent (excitation and emission) properties. X-ray diffraction was performed to examine the crystal structure, grain size, and single-phase formation of the as-prepared nano-products. A comparative Fourier transform infrared (FTIR), Raman spectra, UV/visible absorption spectra, excitation, and emission spectral analysis was presented to authenticate the effect of the host lattice on the photo-physical properties of the materials.

2. Experimental

2.1. Materials

La_2O_3(98%, BDH chemicals, UK), Gd_2O_3(98.8%, BDH chemicals, England), Yttrium oxide (BDH, chemicals, UK), urea, HNO_3, C_2H_5OH were purchased AR grade and employed as received without further purification. All metal oxides were converted into metal nitrates by dissolving in diluted HNO_3. Milli-Q (Millipore, Bedford, USA) H_2O was utilized for the preparation and characterization of the metal phosphate NPs.

2.2. Synthesis of the Eu^{3+}-ion doped metal phosphate nanoparticles

For the preparation of the $LnPO_4$:Eu NPs, freshly prepared 9.5 ml of 2M lanthanum nitrate heptahydrate dissolved in aqueous media, and 0.05 ml 2M europium nitrate hexahydrate were mixed into 100 ml kept on the hot plate for vigorous mechanical stirring at 70 ^oC[22, 23]. 5 g urea liquified in an aqueous media was dropwise injected into an ongoing magnetically stirred reaction mixture for slow thermal decomposition of the metal nitrates into metal carbonates. This reaction proceeded on the hot plate until the homogeneous transparent solution occurred. After that, the reaction was transferred into the reflexing condition at an elevated temperature of 150 ^oC for the complete decay of urea into amine and carbonates. Then an equal volume of sodium dihydrogen phosphate dissolved in an aqueous mixture was dropwise added into the ongoing reaction mixture. This reaction further proceeded for ~5 hrs. Occurred precipitate was separated by centrifugation, washed with H_2O to eliminate the unreacted byproducts, and dried overnight in an oven at 80 ^oC. Similar reaction conditions were employed for the synthesis of $GdPO_4$:Eu and YPO_4:Eu NPs.

2.3. Characterization

Powder XRD pattern (PANalytical X'PERT, Netherland) x-ray diffractometer fitted with Ni filter and Cu Kα (λ=1.5404Å) radiation. FTIR spectra Vertex 80 (Bruker, USA) spectrometer was employed using by KBr pellet procedure in 400-4000 cm^{-1} frequency range. Raman spectra were measured from the (IY-Horiba-T64000) Raman spectrometer at ambient temperature. UV/Visible spectra were recorded from the Cary 60 (Agilent Technologies, USA) spectrophotometer in ethanol in the range of 200-650 nm wavelength. Emission and excitation spectra were measured from the Flourologe-3

(Model FL3-11, Horiba Jobin Yvon, Edison, USA) spectrophotometer. All characteristics of the metal phosphates were carried out under environmental conditions.

3. Results and Discussion

3.1. Crystallographic study

A Powder XRD profile was used to inspect the comparative crystallographic, crystal phase, crystallinity, and phase cleanliness of the as-prepared nano products. As proved in **Fig. 1** the reflection lines' position and intensities in the XRD pattern of the $LaPO_4$:Eu, $GdPO_4$:Eu, and YPO_4:Eu sample were completely matched with the hexagonal structure, which is well-indexed to the JCPDS Card No. 046-1439[24-26], JCPDS card No. 039-0232[21, 27, 28] and JCPDS Card No. 042-0082, respectively[17, 29, 30]. No additional peaks related to the metal oxide or other additives are detected in the entire XRD profile, it endorsed the synthesis of a highly pure, one-phase nanoproduct. Additionally, it suggested that the doped Eu^{3+}-ion was efficiently distributed in the crystal lattice in all three metal phosphate samples. As presented in **Fig. 1a** the width of the diffraction planes in all three metal phosphates samples was highly broad, it indicated the small crystalline size of the particles. In a comparative analysis, a substantial improvement in the diffraction lines intensity in YPO_4:Eu NPs is observed in comparison to the $LaPO_4$:Eu and $GdPO_4$:Eu NPs. Whereas, a slight shift in the reflection peak positions is detected in the YPO_4:Eu NPs than in the $LaPO_4$:Eu and $GdPO_4$:Eu NPs. It assumes that the shifting in the reflection peaks because of the larger ionic radii Eu^{3+}=0.95Å doped into the smaller size ionic radii Y^{3+} crystal lattice Y^{3+}=0.89Å (**Fig. 1b**). It indicated that the substituted Eu^{3+}-ion occupied the Y^{3+} cation positions, therefore the lattice of the crystal was slightly enlarged. The slight enlargement of the host lattice distorts the symmetry because of alterations in the bond angle and bond distances. Causing the symmetry distortion the reflection plane intensities as well as peak positions were shifted in the XRD pattern [31, 32]. Jia et al reported that the ionic radii differences affect the reflection peak positions in the XRD pattern such as doping of the small size ion into bigger ionic radii host lattice shifts the reflection peaks at a higher angle, whereas the bigger ionic radii dopant with smaller size ionic radii ions shift the reflection lines at a lower angle (Y^{3+}=1.019Å, La^{3+}=1.16Å, Eu^{3+}=1.06Å, and Gd^{3+}=1.05Å in eight coordinated)[32]. An observed lattice constant are a = 6.798Å, b= 7.115Å, and c= 6.591Å for the $LaPO_4$:Eu;

a= 6.708Å, b= 7.101Å, and c= 6.482Å for the $GdPO_4$:Eu; and a = 6.831Å, b= 6.175Å, c= 6.652Å for the YPO_4:Eu NPs. The observed lattice parameters are similar to the previous reports [33, 34]. A significant reduction in the calculated lattice parameters was observed it reflects the impact of the variation in the host and doped ions ionic radii [35, 36]. Additionally, the substituted doped ion replaces the host ion causing it to reduce the lattice parameters, which are estimated in the order YPO_4:Eu>$LaPO_4$:Eu> $GdPO_4$:Eu, respectively (**Fig. 1**)[15, 37]. It is anticipated that in luminescent materials higher crystalline phase typically correlates to fewer trapping agents and brighter fluorescence. In the optically active or photosensitive particle crystal structure, particle size plays an important role in enhancing emission efficiency. Better crystalline phase results in fewer both bulk and surface imperfections, which act as photo-induced electron quenching points and reduce luminescence intensity. The average crystalline size of the nanoproducts was assessed from the full-width half maxima of the strongest reflection plane (102) observed at 31.7^o calculated through the Scherrer equation to be 13.9, 14.89, and 18.7 nm for $LaPO_4$:Eu, $GdPO_4$:Eu, and YPO_4:Eu NPs, respectively.

3.2. Surface properties

FTIR spectra were performed to inspect the attachment of the organic and water molecules surrounding the exterior of the nanocrystals. **Fig.2** displays the FTIR spectra of the as-synthesized $LaPO_4$:Eu, $GdPO_4$:Eu, and YPO_4:Eu NPs in a comparative analysis. All FTIR spectrum shows a diffused band in between 300-3600 cm^{-1} attributed to the asymmetric/symmetric stretching vibrational mode of the (O-H) functional group related to the physically or chemically outward adsorbed H_2O particles [29, 38]. Three strong intensity bands located at ~1000-1200, 640, and 550 cm^{-1} are associated with the asymmetric stretching, bending, and wagging vibrational modes of the phosphate group (PO_4^{3-})[39, 40]. These are well-known infrared absorption band in the FTIR spectra, which shows strong intensity because of the higher concentration of the phosphate molecule in the metal phosphate NPs. A sharp with a strong middle-intensity peak at a lower frequency appeared at ~462 cm^{-1}, which is ascribed to the meta-oxygen network[41, 42]. It endorsed the formation of the metal-oxygen framework in the crystal lattice.

3.3. Raman shift

Raman spectra were recorded to estimate the structural dis-order in three Eu^{3+}-ion doped metal phosphate NPs. **Fig. 3** illustrated the comparative Raman spectra of the $LaPO_4$:Eu, $GdPO_4$:Eu, and YPO_4:Eu NPs to distinguish the peak sensitivity and position f the observed Raman vibrational bands[43-45]. Raman spectra of the three samples exhibited two strong broadband located at 811, and 880 cm^{-1}, which are credited to the hexagonal phase of the metal phosphates. The Raman peak intensity was remarkably higher in the $GdPO_4$:Eu NPs in contrast to the $LaPO_4$:Eu and YPO_4:Eu NPs, it may be the impact of the host and guest ion size, which shrinks/enlarge the crystal lattice based on the doped cation ionic radii, as described in the XRD discussion.

3.3. Optical characteristics

Fig. 4 displayed the comparative absorption spectra of the as-synthesized Eu^{3+}-ion doped metal phosphate NPs to explore the optical characteristics, aqueous dispersibility, and colloidal solidity in an aqueous solution. The absorption spectra of the $LaPO_4$:Eu, $GdPO_4$Eu, and YPO_4:Eu NPs in an aqueous solution revealed good absorbance in the ultraviolet region. A strong absorbance in the UV range of the as-prepared NPs specified good dispersibility and colloidal stability. It assumes that the exterior of the metal phosphate NPs is shielded with abundant hydroxyl molecules which assist in the formation of hydrogen bonding through van der Waal force interaction (**Fig. 4**). FTIR spectral results as discussed in the previous section existence of the surface hydroxyl groups, which support the colloidal steadiness of the as-synthesized NPs. Generally, it is expected that the high colloidal dispersibility of the NPs leads to an increase in the biocompatibility and non-toxicity of the metal phosphate NPs.

UV/Visible spectra were exploited to monitor the optical energy bandgap (E_g) of the as-prepared three metal phosphate NPs to understand the optical characteristics and their correlation with the grain size of the ceramic materials. Tauc formulae were employed to regulate the bandgap energy, in which absorption spectra were plotted photon energy ($h\nu$) versus $(\alpha h\nu)^2$ as demonstrated in **Fig. 5**[46]. According to the curve plotted in **Fig. 5**, the straight portion of the curve exhibited the values 5.14, 5.03, and 4.90 eV for the $LaPO_4$:Eu, $GdPO_4$:Eu, and YPO_4:Eu NPs, respectively.

3.4. Photoluminescence properties

Comparative photoluminescence properties were recorded to examine the impact of the host material on the exciton and emission lines of the doped luminescent Eu^{3+}-ion. **Fig. 6** displays the excitation spectrums of the $LaPO_4$:Eu, $GdPO_4$:Eu, and YPO_4:Eu NPs on irradiation of all samples from the 595 nm($^5D_0 \rightarrow {}^7F_1$) emission wavelength. The excitation spectra of the three-metal phosphate exhibited seven 4f-4f intra-configurational exciton located at 312, 317-324, 363, 375, 393, 437, and 465 nm, which correspond to $^7F_0 \rightarrow {}^5I_6$, $^7F_{0,1} \rightarrow {}^5H_{3,6}$, $^7F_{0,1} \rightarrow {}^5D_4$, $^7F_{0,1} \rightarrow {}^5G_3$, $^7F_{0,1} \rightarrow {}^5L_6$, $^7F_{0,1} \rightarrow {}^5D_3$, and $^7F_{0,1} \rightarrow {}^5D_2$ of the Eu^{3+}-ion, respectively (**Fig. 6**). In a comparative analysis a substantial improvement in the exciton transitions sensitivity was observed in comparison to the $LaPO_4$:Eu, and YPO_4:Eu NPs. Although, the exciton intensity was greater in YPO_4:Eu NPs than in the $LaPO_4$:Eu NPs. An observed intensity in the three metal phosphate NPs is in order $GdPO_4$:Eu>YPO_4:Eu>$LaPO_4$:Eu NPs. As illustrated in **Fig. 6** the intensity of the exciton transitions in the case $LaPO_4$:Eu NPs is very weak in contrast to the $GdPO_4$:Eu and YPO_4:Eu NPs. It depends on the charge transfer and crystallinity of the host lattice, which assists in promoting the luminescent efficiency of the doped luminescent center ions.

Emission spectra were measured on excitation of the all three metal phosphate NPs on a similar excitation wavelength to accurately define the impact of the host lattice. Emission spectra were monitored under excitation from the e_x=393 nm wavelength in the range from 450-750 nm wavelength as shown in **Fig. 7a&b**. The emission spectra in **Fig.7** demonstrated the most intensive luminescence lines located at 467, 534, 590, 612, 644, and 696 nm, which are labeled as $^5D_1 \rightarrow {}^7F_1$, $^5D_1 \rightarrow {}^7F_3$, $^5D_0 \rightarrow {}^7F_1$, $^5D_0 \rightarrow {}^7F_2$, $^5D_0 \rightarrow {}^7F_3$, and $^5D_0 \rightarrow {}^7F_4$, of the 4f-4f intra-configurational Eu^{3+}-ion most emissive transitions, respectively[39]. The emission spectra of the three metal phosphate NPs display the two most intensive emission transitions in the middle of the spectrum, which are assigned as $^5D_0 \rightarrow {}^7F_1$ magnetic-dipole, and $^5D_0 \rightarrow {}^7F_2$ electric-dipole emission lines. The magnetic-dipole and electric dipole transition play a significant role in distinguishing the crystal phase relationship and also determining the degree of alteration from the inversion symmetry. Generally, it is fact that the electric-dipole ($^5D_0 \rightarrow {}^7F_2$) emission line is an

electronically allowed transition, therefore, it is immensely effective in the coordination with surrounding chemical groups around the Eu^{3+}-ion. Whereas the magnetic-dipole ($^5D_0 \rightarrow {}^7F_1$) emission line is unresponsive, it barely alters crystal field intensity nearby the Eu^{3+}-ion. The most noticeable emission peak is the so-called hypersensitive red luminescent transition, which is positioned at 612 nm ($^5D_0 \rightarrow {}^7F_2$). The electric dipole ($^5D_0 \rightarrow {}^7F_2$) transition is more robust than the corresponding magnetic-dipole ($^5D_0 \rightarrow {}^7F_1$) transition in the luminescent spectrum if the Eu^{3+}-ion is in a low symmetry location, which indicates it lacks an inversion center[47, 48]. However, the position symmetry at which place the Eu^{3+}-ion is located does not affect the magnetic dipole ($^5D_0 \rightarrow {}^7F_1$) transition [33]. The luminescence spectra of the $GdPO_4$:Eu and YPO_4:Eu NPs illustrated the most sensitive electric dipole ($^5D_0 \rightarrow {}^7F_2$) emission transition[21, 49]. In which, magnetic-dipole ($^5D_0 \rightarrow {}^7F_1$) emission transition is less sensitive as exhibited in **Fig. 7a&b**. It implies that the doped Eu^{3+}-ion in the $GdPO_4$ and YPO_4 crystal matrix are present in the asymmetric position in both host materials[20, 28]. The luminescence efficiency of these transitions defines the quality of the host matrix, which is the most useful technique to identify and development of the particular laser diode, and further their usage in luminescent-based applications such as optical bio-probe, bio-detection, and optical biosensors. Dong et al., described that a perfect red luminescent material should emit a red laser from the electric dipole ($^5D_0 \rightarrow {}^7F_2$) emission line despite having little orange light from the magnetic-dipole ($^5D_0 \rightarrow {}^7F_1$) emission line[50].

Although in the case of $LaPO_4$:Eu NPs magnetic-dipole and electric-dipole, both transitions showed equal sensitivity, even though, the efficiency of the magnetic-dipole emission transition is slightly greater in comparison to the electric-dipole transition, it endorsed that the Eu^{3+}-ion exists in the host lattice in inversion symmetry with C_1 space group. These results are quite similar to the previous reports [13, 24, 44]. Rambabu et al. described that the enhancement in the magnetic-dipole ($^5D_0 \rightarrow {}^7F_1$) emission peak in contrast to the electric-dipole ($^5D_0 \rightarrow {}^7F_2$) emission peak caused the easy charge transfer between the host and doped cations[51]. Similar observations were reported by Yu et al., an alteration in the emission intensity of the two most sensitive luminescence transitions of Eu^{3+}-ion[52]. Despite low-temperature preparation, the primary Eu^{3+} positions symmetry is similar to that of the macro-size material[53]. As exhibited in **Fig.7**

the intensity ratio of the emission transitions indicated that a large number of Eu^{3+} ions inhibit the inversion position in the $LaPO_4$:Eu NPs[23, 54]. It is an actual technique to measure the efficiency and purity of the as-prepared metal phosphate NPs because the localized symmetry of the inserted Eu^{3+}-ion in the host material has a significant impact on how sensitive these luminescence transitions are[22]. The host lattice diameter, shape, crystal phase, and lattice locations for Eu^{3+} ions are significant variables that significantly distress luminescent efficiency. The La^{3+} site that exhibits C_1 point group symmetry in the monoclinic crystal structure of $LaPO_4$ has non-inversion symmetry[13, 23].

It is fact that due to small atomic size differences, Eu^{3+} ions (1.06Å) and La^{3+} ions (1.16Å) can both occupy the same locations in a crystal. The emission efficacy of the materials is greatly influenced by the excellent crystallinity and crystal shape of the ceramic materials[23]. It is a proven fact that good crystalline structure constantly favors increasing emission and excitation efficiency. Small grains and a large surface area allow for easy H_2O molecule adsorption on their exterior, which also allows for the coordination of organic moieties. Considering that metal phosphate NPs are made in an aqueous solvent and that hydroxyl groups may be present on their surface, these findings are also supported by the observed FTIR spectral results. Because abundant functional molecules are soaked on the exterior of metal phosphate nanocrystals, their surface properties are distinct from those of bulk counterparts. These surfaces adsorbed high vibrational energy either H_2O or other organic functional group molecules quenched the luminescence intensity at a large scale. These exterior-anchored crystal imperfections (trap centers) may also function as non-radiative recombination trap molecules that are accountable for suppressing the emission efficiency of the materials. Furthermore, these outcomes were also sustained from the emission spectra of all three metal phosphates. As observed in **Fig.7**, the emission spectra display a feeble intensity of the emission transition situated at ~534 nm corresponds to the ($^5D_1 \rightarrow {}^7F_1$) transition, which seems caused by the $LnPO_4$ host lattice's low vibrational energy (350 cm^{-1}). This finding suggests that the host material protects the Eu^{3+} ion from the nearby H_2O molecules, because high phonon energy (3500 cm^{-1}) molecules, effectively quenched the emission efficiency of the doped luminescent ion.

In a comparative spectral study, the emission transitions in the $GdPO_4$:Eu NPs are significantly highly sensitive in comparison to the YPO_4:Eu and $LaPO_4$:Eu NPs[29]. It is fact that the Gd^{3+} ion displays strong absorption transition located at ~250, and 270 nm assigned to $^8S \rightarrow {}^6D$ and $^8S_{7/2} \rightarrow {}^6I_j$ transitions overlap on the $^5D_0$ level of the Eu^{3+} ion as appeared in the luminescent spectrums, that effectively charge transfer from Gd^{3+}-ion to the doped Eu^{3+}-ion leading to enhance the emission efficiency, similar observations also reported in a previous report(**Fig.7b**) [16, 24]. Because yttrium and lanthanum both are diamagnetic because their 4d subshell is filled and the absence of the 4f-subshell. But the observed emission spectral results suggested that the $LaPO_4$ is not a suitable host for doping of the Eu^{3+}-ion in comparison to the $GdPO_4$ and YPO_4 host lattice. However, the emission and excitation finding suggested that the $GdPO_4$:Eu^{3+} is the best host matrix for producing excellent emission efficiency.

4. Conclusion

Eu^{3+}-doped metal phosphate NPs were synthesized to examine the effect of the host lattice on physiochemical, and luminescent characteristics. The sensitivity of the reflection peaks, peak positions, lattice parameters, and crystallinity confirmed that the doping of the luminescent Eu^{3+}-ion disturbed the crystal symmetry, because of the difference between the host and doped cation ionic radii. The bond angle and bond length shrink in the case of small-size doped ions, whereas, the crystal lattice enlarges in bigger-size ionic radii doped cation. FTIR spectra verified the presence of the phosphate group and hydroxyl group IR vibrational bands. A significant absorption band intensity even shifting in band edge was observed it certified the good colloidal dispersibility in aqueous solution. Raman shift and bandgap energy reflected the presence of Raman active modes and optical activity in the UV/visible region. The emission and excitation transitions were dominant in the order $GdPO_4$:Eu > YPO_4:Eu > $LaPO_4$:Eu NPs, respectively. The high sensitivity of the excitation and emission transitions in the $GdPO_4$:Eu NPs because of the easy charge transfer process between the Gd^{3+}-ion and Eu^{3+}-ion. Although, the sensitivity of the magnetically-dipole transition and electric-dipole transition were highly affected in all three metal phosphate samples in comparison to the conversational metal oxide host

lattices. Based on the observed results, $GdPO_4$:Eu NPs are highly useful in luminescent-based biotechnological applications.

Acknowledgment: The author is thankful to the Researchers Supporting Project number (RSP2023R365), King Saud University, Riyadh, Saudi Arabia

Conflict of interest The authors declare that they have no known competing financial interests or personal relationships that could have appeared to influence the work reported in this paper.

References

[1] Y. Fan, F. Zhang, A New Generation of NIR-II Probes: Lanthanide-Based Nanocrystals for Bioimaging and Biosensing, Adv Opt Mater 7(7) (2019) 1801417.
[2] A.A. Ansari, V.K. Thakur, G. Chen, Functionalized upconversion nanoparticles: New strategy towards FRET-based luminescence bio-sensing, Coordination Chemistry Reviews 436 (2021) 213821.
[3] A.A. Ansari, A.K. Parchur, N.D. Thorat, G. Chen, New advances in pre-clinical diagnostic imaging perspectives of functionalized upconversion nanoparticle-based nanomedicine, Coordination Chemistry Reviews 440 (2021) 213971.
[4] S.K. Gupta, J.P. Zuniga, M. Abdou, M.P. Thomas, M.D. Goonatilleke, B.S. Guiton, Y.B. Mao, Lanthanide-doped lanthanum hafnate nanoparticles as multicolor phosphors for warm white lighting and scintillators, Chemical Engineering Journal 379 (2020).
[5] W. Ren, G. Lin, C. Clarke, J. Zhou, D. Jin, Optical Nanomaterials and Enabling Technologies for High-Security-Level Anticounterfeiting, Adv Mater 32(18) (2020) 1901430.
[6] M.Q. Tan, Z.Q. Ye, G.L. Wang, J.L. Yuan, Preparation and time-resolved fluorometric application of luminescent europium nanoparticles, Chemistry of Materials 16(12) (2004) 2494-2498.
[7] Z.Q. Ye, M.Q. Tan, G.L. Wang, J.L. Yuan, Novel fluorescent europium chelate-doped silica nanoparticles: preparation, characterization and time-resolved fluorometric application, Journal of Materials Chemistry 14(5) (2004) 851-856.
[8] A.A. Ansari, M.R. Muthumareeswaran, R. Lv, Coordination chemistry of the host matrices with dopant luminescent Ln3+ ion and their impact on luminescent properties, Coordination Chemistry Reviews 466 (2022) 214584.
[9] G.Y. Chen, H.L. Qju, P.N. Prasad, X.Y. Chen, Upconversion Nanoparticles: Design, Nanochemistry, and Applications in Theranostics, Chemical Reviews 114(10) (2014) 5161-5214.
[10] A.A. Ansari, A.K. Parchur, G. Chen, Surface modified lanthanide upconversion nanoparticles for drug delivery, cellular uptake mechanism, and current challenges in NIR-driven therapies, Coordination Chemistry Reviews 457 (2022) 214423.
[11] W.B. Bu, L.X. Zhang, Z.L. Hua, H.R. Chen, J.L. Shi, Synthesis and characterization of uniform spindle-shaped microarchitectures self-assembled from aligned single-crystalline nanowires of lanthanum phosphates, Crystal Growth & Design 7(11) (2007) 2305-2309.
[12] Z.X. Fu, W.B. Bu, High efficiency green-luminescent LaPO4 : Ce,Tb hierarchical nanostructures: Synthesis, characterization, and luminescence properties, Solid State Sciences 10(8) (2008) 1062-1067.

[13] H. Lai, A. Bao, Y.M. Yang, Y.C. Tao, H. Yang, Selective synthesis and luminescence property of monazite- and hexagonal-type LaPO4: Eu nanocrystals, Crystengcomm 11(6) (2009) 1109-1113.
[14] A.K. Gulnar, V. Sudarsan, R.K. Vatsa, T. Sakuntala, A.K. Tyagi, U.K. Gautam, A. Vinu, Nucleation sequence on the cation exchange process between Y0.95Eu0.05PO4 and CePO4 nanorods, Nanoscale 2(12) (2010) 2847-2854.
[15] T. Grzyb, R.J. Wiglusz, A. Gruszeczka, S. Lis, Down- and up-converting dual-mode YPO4:Yb3+,Tb3+ nanocrystals: synthesis and spectroscopic properties, Dalton T 43(46) (2014) 17255-17264.
[16] S. Rodriguez-Liviano, A.I. Becerro, D. Alcantara, V. Grazu, J.M. de la Fuente, M. Ocana, Synthesis and Properties of Multifunctional Tetragonal Eu:GdPO4 Nanocubes for Optical and Magnetic Resonance Imaging Applications, Inorganic Chemistry 52(2) (2013) 647-654.
[17] M.N. Luwang, R.S. Ningthoujam, Jagannath, S.K. Srivastava, R.K. Vatsa, Effects of Ce3+ Codoping and Annealing on Phase Transformation and Luminescence of Eu3+-Doped YPO4 Nanorods: D2O Solvent Effect, Journal of the American Chemical Society 132(8) (2010) 2759-2768.
[18] A.K. Parchur, A.I. Prasad, S.B. Rai, R.S. Ningthoujam, Improvement of blue, white and NIR emissions in YPO4:Dy3+ nanoparticles on co-doping of Li+ ions, Dalton T 41(45) (2012) 13810-13814.
[19] M.N. Luwang, R.S. Ningthoujam, S.K. Srivastava, R.K. Vatsa, Disappearance and Recovery of Luminescence in Bi3+, Eu3+ Codopecl YPO4 Nanoparticles Due to the Presence of Water Molecules Up to 800 degrees C, Journal of the American Chemical Society 133(9) (2011) 2998-3004.
[20] L.H. Zhang, G. Jia, H.P. You, K. Liu, M. Yang, Y.H. Song, Y.H. Zheng, Y.J. Huang, N. Guo, H.J. Zhang, Sacrificial Template Method for Fabrication of Submicrometer-Sized YPO4:Eu3+ Hierarchical Hollow Spheres, Inorganic Chemistry 49(7) (2010) 3305-3309.
[21] L.H. Zhang, M.L. Yin, H.P. You, M. Yang, Y.H. Song, Y.J. Huang, Mutifuntional GdPO4:Eu3+ Hollow Spheres: Synthesis and Magnetic and Luminescent Properties, Inorganic Chemistry 50(21) (2011) 10608-10613.
[22] S.K. Gupta, P.S. Ghosh, M. Sahu, K. Bhattacharyya, R. Tewari, V. Natarajan, Intense red emitting monoclinic LaPO4:Eu3+ nanoparticles: host-dopant energy transfer dynamics and photoluminescence properties, Rsc Adv 5(72) (2015) 58832-58842.
[23] G. Phaomei, R.S. Ningthoujam, W.R. Singh, N.S. Singh, M.N. Luwang, R. Tewari, R.K. Vatsa, Low temperature synthesis and luminescence properties of re-dispersible Eu3+ doped LaPO4 nanorods by ethylene glycol route, Optical Materials 32(5) (2010) 616-622.
[24] V. Buissette, M. Moreau, T. Gacoin, J.P. Boilot, J.Y. Chane-Ching, T. Le Mercier, Colloidal synthesis of luminescent rhabdophane LaPO4 : Ln(3+)center dot xH(2)O (Ln = Ce, Tb, Eu; x approximate to 0.7) nanocrystals, Chemistry of Materials 16(19) (2004) 3767-3773.
[25] Y.W. Zhang, Z.G. Yan, L.P. You, R. Si, C.H. Yan, General synthesis and characterization of monocrystalline lanthanide orthophosphate nanowires, European Journal of Inorganic Chemistry (22) (2003) 4099-4104.
[26] M. Runowski, T. Grzyb, A. Zep, P. Krzyczkowska, E. Gorecka, M. Giersig, S. Lis, Eu3+ and Tb3+ doped LaPO4 nanorods, modified with a luminescent organic compound, exhibiting tunable multicolour emission, Rsc Adv 4(86) (2014) 46305-46312.
[27] W.L. Ren, G. Tian, L.J. Zhou, W.Y. Yin, L. Yan, S. Jin, Y. Zu, S.J. Li, Z.J. Gu, Y.L. Zhao, Lanthanide ion-doped GdPO4 nanorods with dual-modal bio-optical and magnetic resonance imaging properties, Nanoscale 4(12) (2012) 3754-3760.

[28] N.K. Sahu, R.S. Ningthoujam, D. Bahadur, Disappearance and recovery of luminescence in GdPO4:Eu3+ nanorods: Propose to water/OH center dot release under near infrared and gamma irradiations, Journal of Applied Physics 112(1) (2012).
[29] H. Lai, Y. Du, M. Zhao, K.N. Sun, L. Yang, Effects of different organic additives on the formation of YPO4:Eu3+ nano-/microstructures under hydrothermal conditions with enhanced photoluminescence, Ceramics International 40(1) (2014) 1885-1891.
[30] C.X. Li, Z.Y. Hou, C.M. Zhang, P.P. Yang, G.G. Li, Z.H. Xu, Y. Fan, J. Lin, Controlled Synthesis of Ln(3+) (Ln = Tb, Eu, Dy) and V5+ Ion-Doped YPO4 Nano-/Microstructures with Tunable Luminescent Colors, Chemistry of Materials 21(19) (2009) 4598-4607.
[31] P.P. Yang, S.L. Gai, Y.C. Liu, W.X. Wang, C.X. Li, J. Lin, Uniform Hollow Lu2O3:Ln (Ln = Eu3+, Tb3+) Spheres: Facile Synthesis and Luminescent Properties, Inorg Chem 50(6) (2011) 2182-2190.
[32] G.A. Jia, H.P. You, Y.H. Song, Y.J. Huang, M. Yang, H.J. Zhang, Facile Synthesis and Luminescence of Uniform Y2O3 Hollow Spheres by a Sacrificial Template Route, Inorganic Chemistry 49(17) (2010) 7721-7725.
[33] N. Yaiphaba, R.S. Ningthoujam, N.S. Singh, R.K. Vatsa, N.R. Singh, S. Dhara, N.L. Misra, R. Tewari, Luminescence, lifetime, and quantum yield studies of redispersible Eu3+-doped GdPO4 crystalline nanoneedles: Core-shell and concentration effects, Journal of Applied Physics 107(3) (2010).
[34] A.K. Parchur, G.S. Okram, R.A. Singh, R. Tewari, L. Pradhan, R.K. Vatsa, R.S. Ningthoujam, Effect Of EDTA On Luminescence Property Of Eu+3 Doped YPO4 Nanoparticles, International Conference on Physics of Emerging Functional Materials (Pefm-2010) 1313 (2010) 391-+.
[35] G. Phaomei, R.S. Ningthoujam, W.R. Singh, R.S. Loitongbam, N.S. Singh, A. Rath, R.R. Juluri, R.K. Vatsa, Luminescence switching behavior through redox reaction in Ce3+ co-doped LaPO4:Tb3+ nanorods: Re-dispersible and polymer film, Dalton Transactions 40(43) (2011) 11571-11580.
[36] C.C. Yu, M. Yu, C.X. Li, X.M. Liu, J. Yang, P.P. Yang, J. Lin, Facile sonochemical synthesis and photoluminescent properties of lanthanide orthophosphate nanoparticles, J Solid State Chem 182(2) (2009) 339-347.
[37] H.J. Song, L.Q. Zhou, L. Li, T. Wang, F. Hong, X.R. Luo, EDTA-assisted hydrothermal synthesis, characterization, and luminescent properties of YPO4 center dot nH(2)O:Eu3+ (n=0, 0.8) microflakes and microbundles, Materials Science and Engineering B-Advanced Functional Solid-State Materials 178(16) (2013) 1012-1018.
[38] G. Phaomei, W.R. Singh, R.S. Ningthoujam, Solvent effect in monoclinic to hexagonal phase transformation in LaPO4:RE (RE=Dy3+, Sm3+) nanoparticles: Photoluminescence study, Journal of Luminescence 131(6) (2011) 1164-1171.
[39] A.A. Ansari, Photochemical studies of monodispersed YPO4:Eu microspheres: The role of surface modification on structural and luminescence properties, J Photoch Photobio A 343 (2017) 126-132.
[40] A.A. Ansari, J.P. Labis, M.A. Manthrammel, Designing of luminescent GdPO4:Eu@LaPO4@SiO2 core/shell nanorods: Synthesis, structural and luminescence properties, Solid State Sciences 71 (2017) 117-122.
[41] A.A. Ansari, M.A.M. Khan, Structural and spectroscopic studies of LaPO4:Ce/Tb@LaPO4@SiO2 nanorods: Synthesis and role of surface coating, Vib Spectrosc 94 (2018) 43-48.
[42] A.A. Ansari, Silica-modified luminescent LaPO4:Eu@LaPO4@SiO2 core/shell nanorods: Synthesis, structural and luminescent properties, Luminescence 33(1) (2018) 112-118.

[43] Q.J. Du, Z.B. Huang, Z. Wu, X.W. Meng, G.F. Yin, F.B. Gao, L. Wang, Facile preparation and bifunctional imaging of Eu-doped GdPO4 nanorods with MRI and cellular luminescence, Dalton Transactions 44(9) (2015) 3934-3940.
[44] M. Saraf, P. Kumar, G. Kedawat, J. Dwivedi, S.A. Vithayathil, N. Jaiswal, B.A. Kaipparettu, B.K. Gupta, Probing Highly Luminescent Europium-Doped Lanthanum Orthophosphate Nanorods for Strategic Applications, Inorganic Chemistry 54(6) (2015) 2616-2625.
[45] M.T. Colomer, J. Bartolomé, A.L. Ortiz, A. de Andrés, Raman characterization and photoluminescence properties of La1-xTbxPO4·nH2O and La1-xTbxPO4 phosphor nanorods prepared by microwave-assisted hydrothermal synthesis, Ceramics International 43(14) (2017) 10840-10847.
[46] J. Tauc, A. Menth, States in the gap, Journal of Non-Crystalline Solids 8-10 (1972) 569-585.
[47] J.J.H.A. van Hest, G.A. Blab, H.C. Gerritsen, C.D. Donega, A. Meijerink, Probing the Influence of Disorder on Lanthanide Luminescence Using Eu-Doped LaPO4 Nanoparticles, J Phys Chem C 121(35) (2017) 19373-19382.
[48] J.W. Stouwdam, G.A. Hebbink, J. Huskens, F.C.J.M. van Veggel, Lanthanide-doped nanoparticles with excellent luminescent properties in organic media, Chem Mater 15(24) (2003) 4604-4616.
[49] A.I. Prasad, A.K. Parchur, R.R. Juluri, N. Jadhav, B.N. Pandey, R.S. Ningthoujam, R.K. Vatsa, Bi-functional properties of Fe3O4@YPO4:Eu hybrid nanoparticles: hyperthermia application, Dalton T 42(14) (2013) 4885-4896.
[50] Q.Z. Dong, Y.H. Wang, L.L. Peng, H.J. Zhang, B.T. Liu, Controllable morphology and high photoluminescence of (Y, Gd)(V, P) O-4:Eu3+ nanophosphors synthesized by two-step reactions, Nanotechnology 22(21) (2011).
[51] U. Rambabu, S. Buddhudu, Optical properties of LnPO4:Eu3+ (Ln=Y, La and Gd) powder phosphors, Opt Mater 17(3) (2001) 401-408.
[52] L. Yu, H. Song, S. Lu, Z. Liu, L. Yang, X. Kong, Luminescent Properties of LaPO4:Eu Nanoparticles and Nanowires, The Journal of Physical Chemistry B 108(43) (2004) 16697-16702.
[53] M. Ferhi, K. Horchani-Naifer, M. Ferid, Combustion synthesis and luminescence properties of LaPO4: Eu (5%), Journal of Rare Earths 27(2) (2009) 182-186.
[54] X.W. Zhang, M.F. Zhang, Y.C. Zhu, P.F. Wang, F. Xue, J. Gu, H.Y. Bi, Y.T. Qian, Hydrothermal synthesis and luminescent properties of LaPO4:Eu 3D microstructures with controllable phase and morphology, Materials Research Bulletin 45(9) (2010) 1324-1329.

Figures and captions

Figure 1.(a&b)X-ray diffraction pattern of the $LaPO_4$:Eu, $GdPO_4$:Eu, and YPO_4:Eu NPs.

Figure 2. FTIR spectra of the $LaPO_4$:Eu, $GdPO_4$:Eu, and YPO_4:Eu NPs.

Figure 3. FT-Raman spectra of the $LaPO_4$:Eu, $GdPO_4$:Eu, and YPO_4:Eu NPs.

Figure 4. UV/Visible absorption spectra of the $LaPO_4$:Eu, $GdPO_4$:Eu, and YPO_4:Eu NPs.

Figure 5. Optical energy bandgap of the $LaPO_4$:Eu, $GdPO_4$:Eu, and YPO_4:Eu NPs.

Figure 6. Excitation spectra of the $LaPO_4$:Eu, $GdPO_4$:Eu, and YPO_4:Eu NPs.

Figure 7. (a&b) Emission spectra of the $LaPO_4$:Eu, $GdPO_4$:Eu, and YPO_4:Eu NPs.

Figure 1

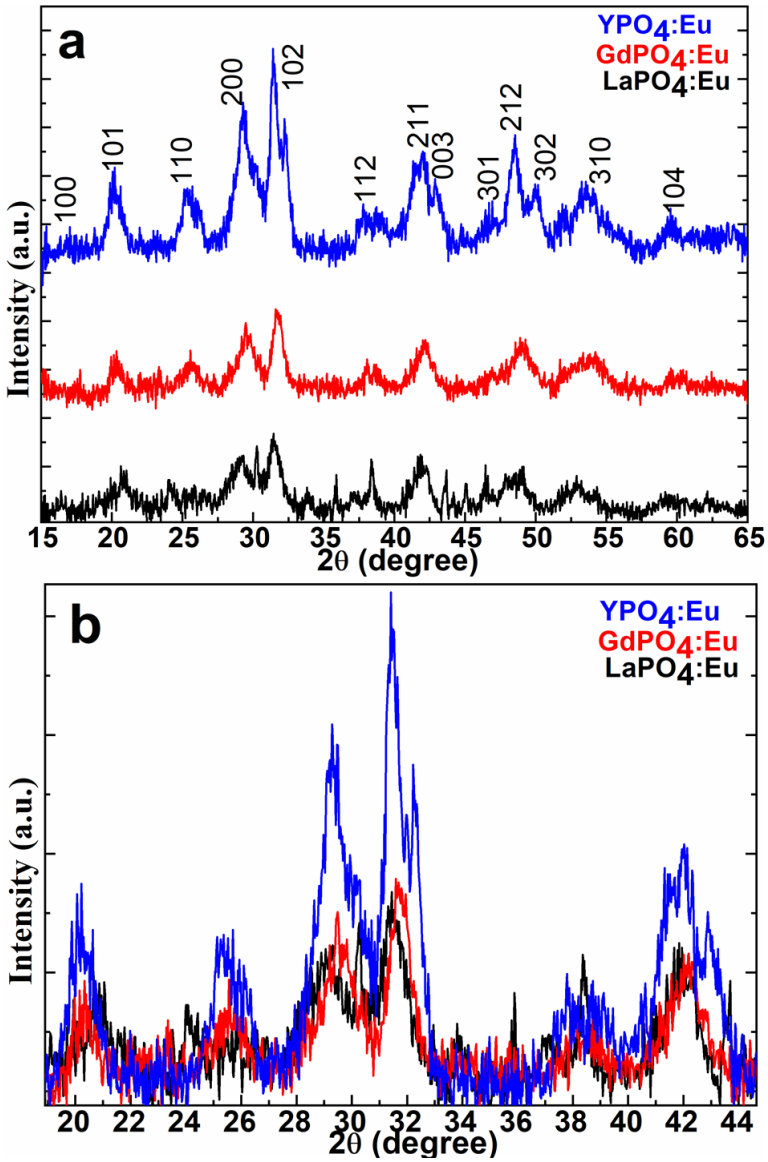
a
YPO4:Eu
GdPO4:Eu
LaPO4:Eu
100
101
110
200
102
112
211
003
301
212
302
310
104
Intensity (a.u.)
15 20 25 30 35 40 45 50 55 60 65
2θ (degree)
b
YPO4:Eu
GdPO4:Eu
LaPO4:Eu
Intensity (a.u.)
20 22 24 26 28 30 32 34 36 38 40 42 44
2θ (degree)

Figure 2

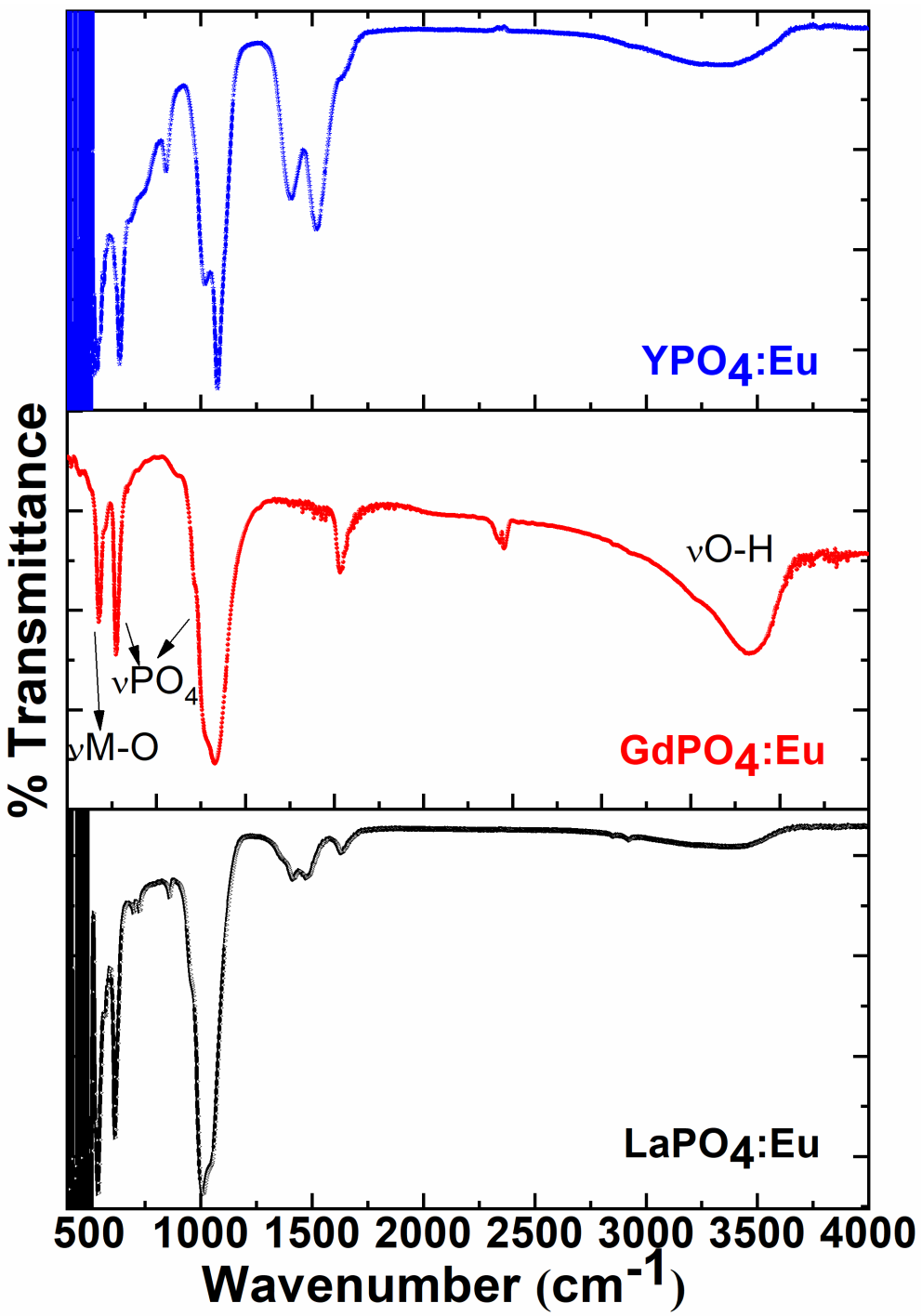
YPO4:Eu
νO-H
νPO4
νM-O
GdPO4:Eu
LaPO4:Eu
% Transmittance
500 1000 1500 2000 2500 3000 3500 4000
Wavenumber (cm-1)

Figure 3

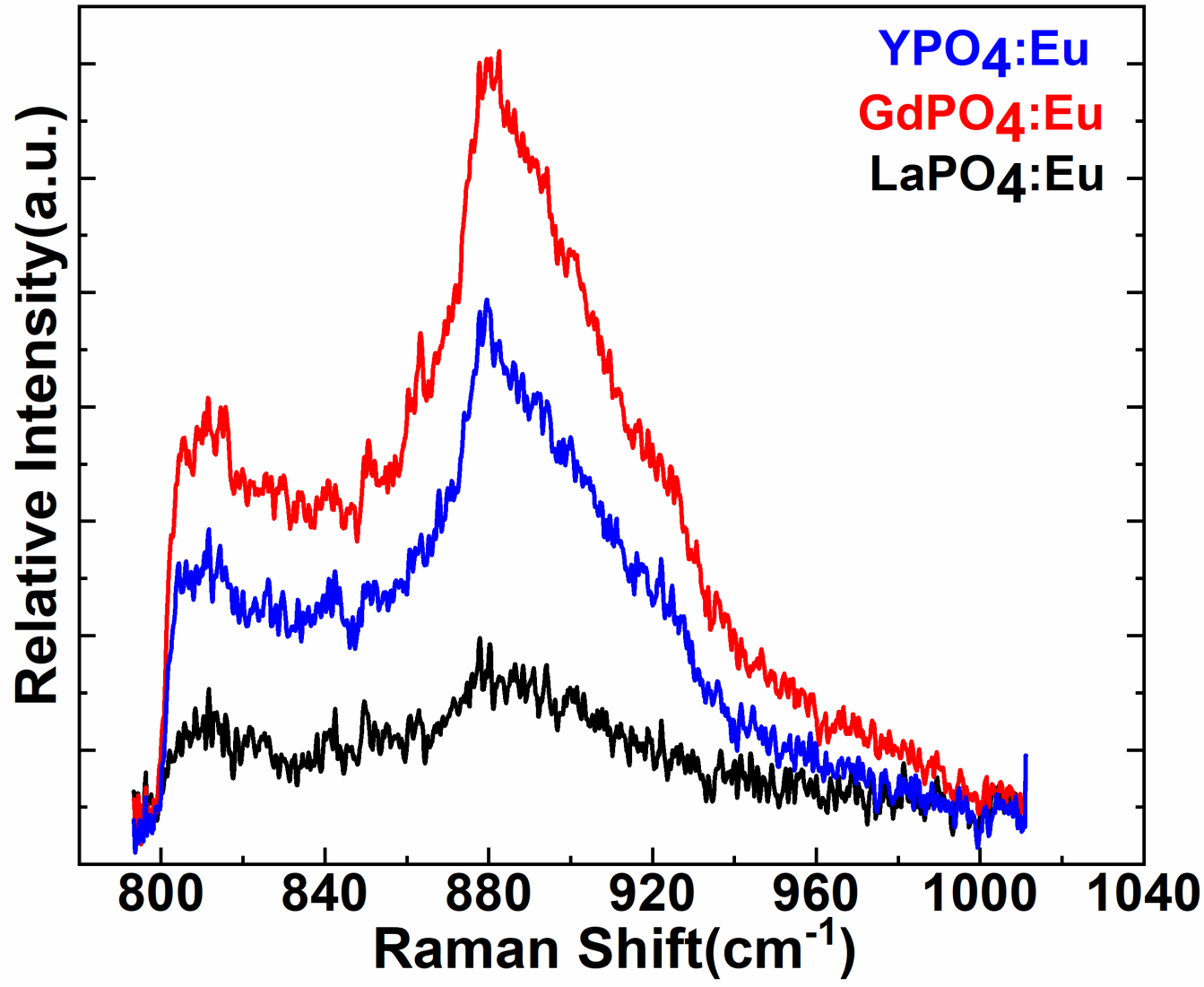
YPO4:Eu
GdPO4:Eu
LaPO4:Eu
Relative Intensity(a.u.)
800
840
880
920
960
1000
1040
Raman Shift(cm-1)

Figure 4

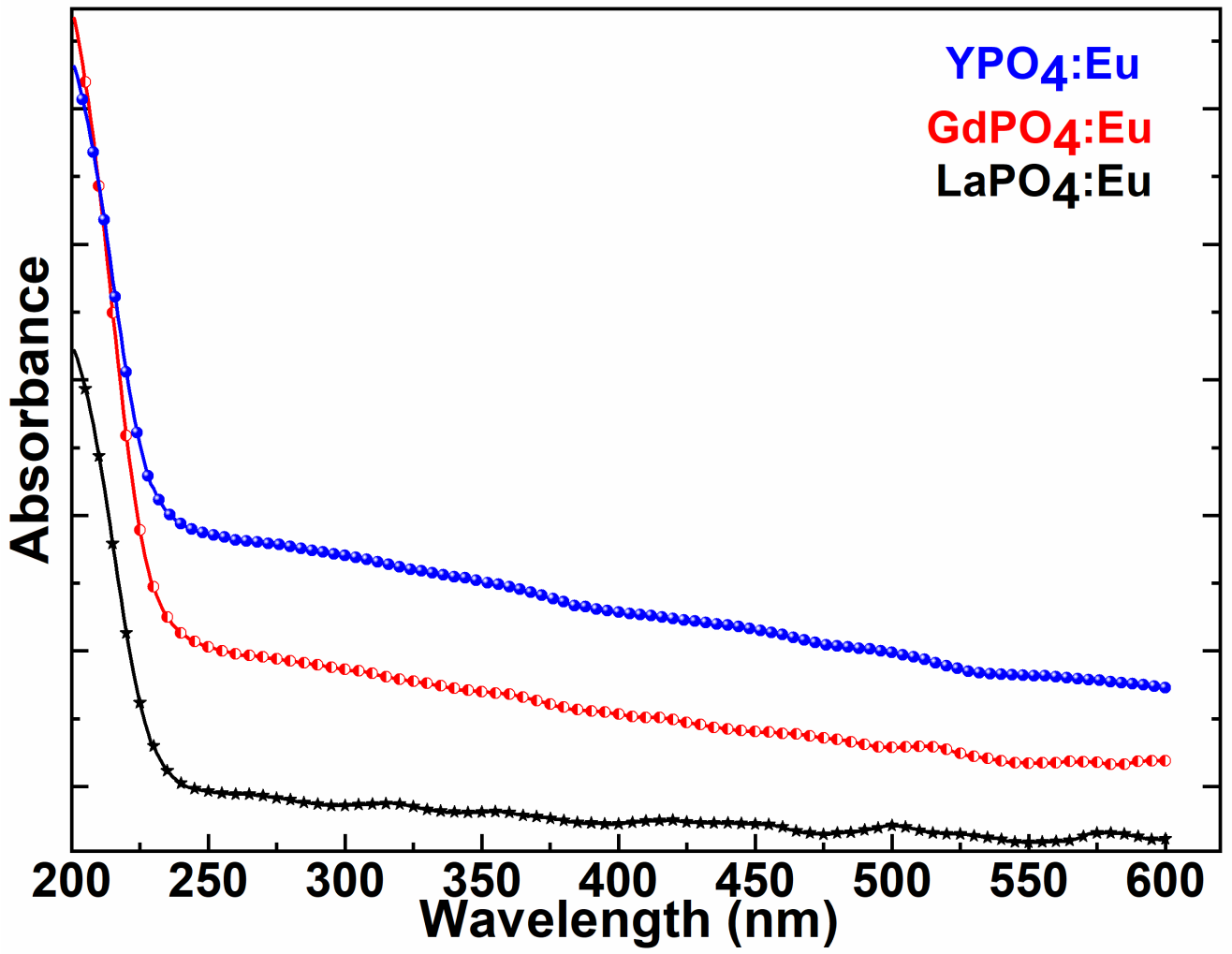

Figure 5

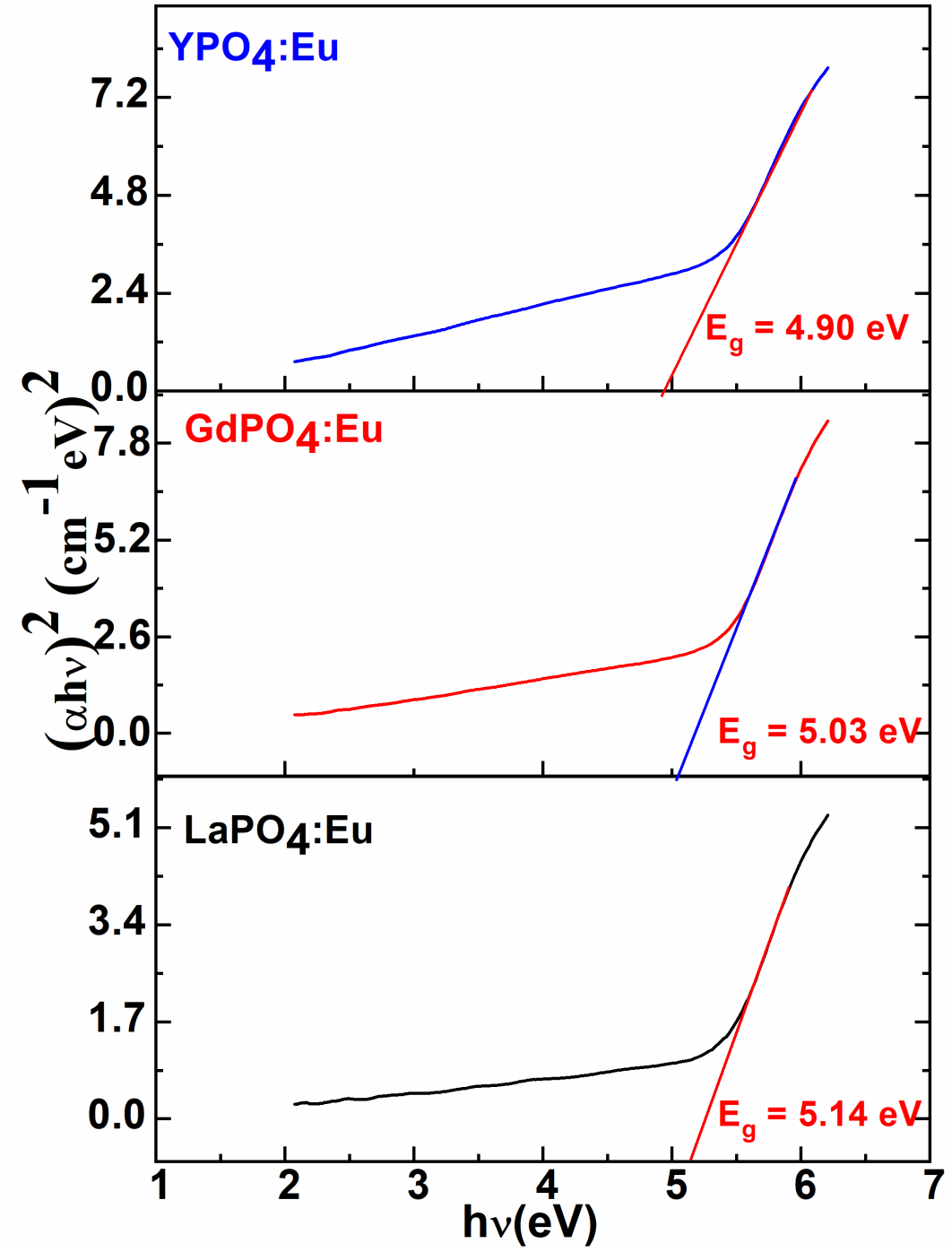
YPO4:Eu
Eg = 4.90 eV
GdPO4:Eu
Eg = 5.03 eV
LaPO4:Eu
Eg = 5.14 eV
(αhν)2 (cm-1eV)2
hν(eV)
7.2
4.8
2.4
0.0
7.8
5.2
2.6
0.0
5.1
3.4
1.7
0.0
1
2
3
4
5
6
7

Figure 6

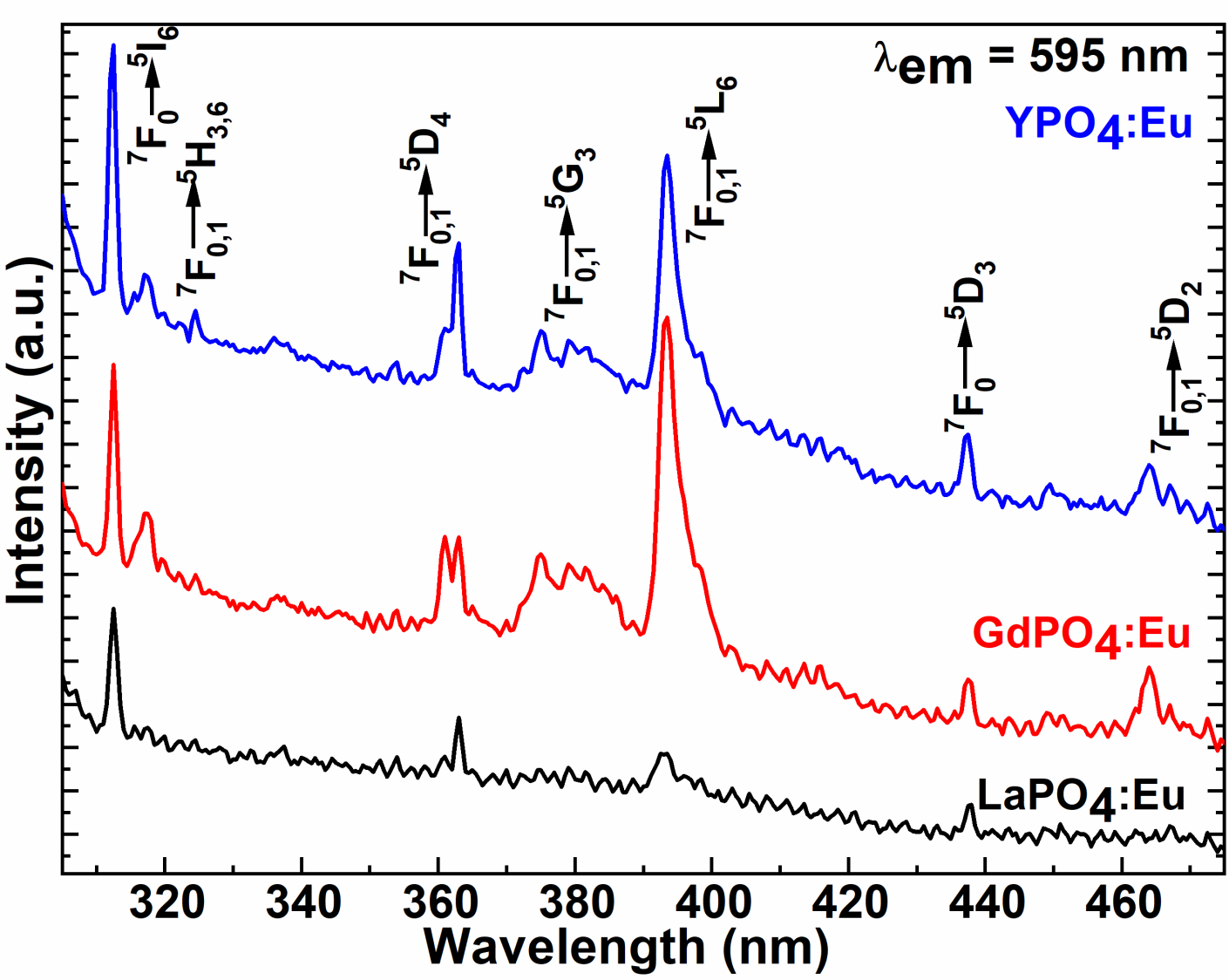
λem = 595 nm
YPO4:Eu
GdPO4:Eu
LaPO4:Eu
7F0 → 5I6
7F0,1 → 5H3,6
7F0,1 → 5D4
7F0,1 → 5G3
7F0,1 → 5L6
7F0 → 5D3
7F0,1 → 5D2
Intensity (a.u.)
Wavelength (nm)
320
340
360
380
400
420
440
460

Figure 7

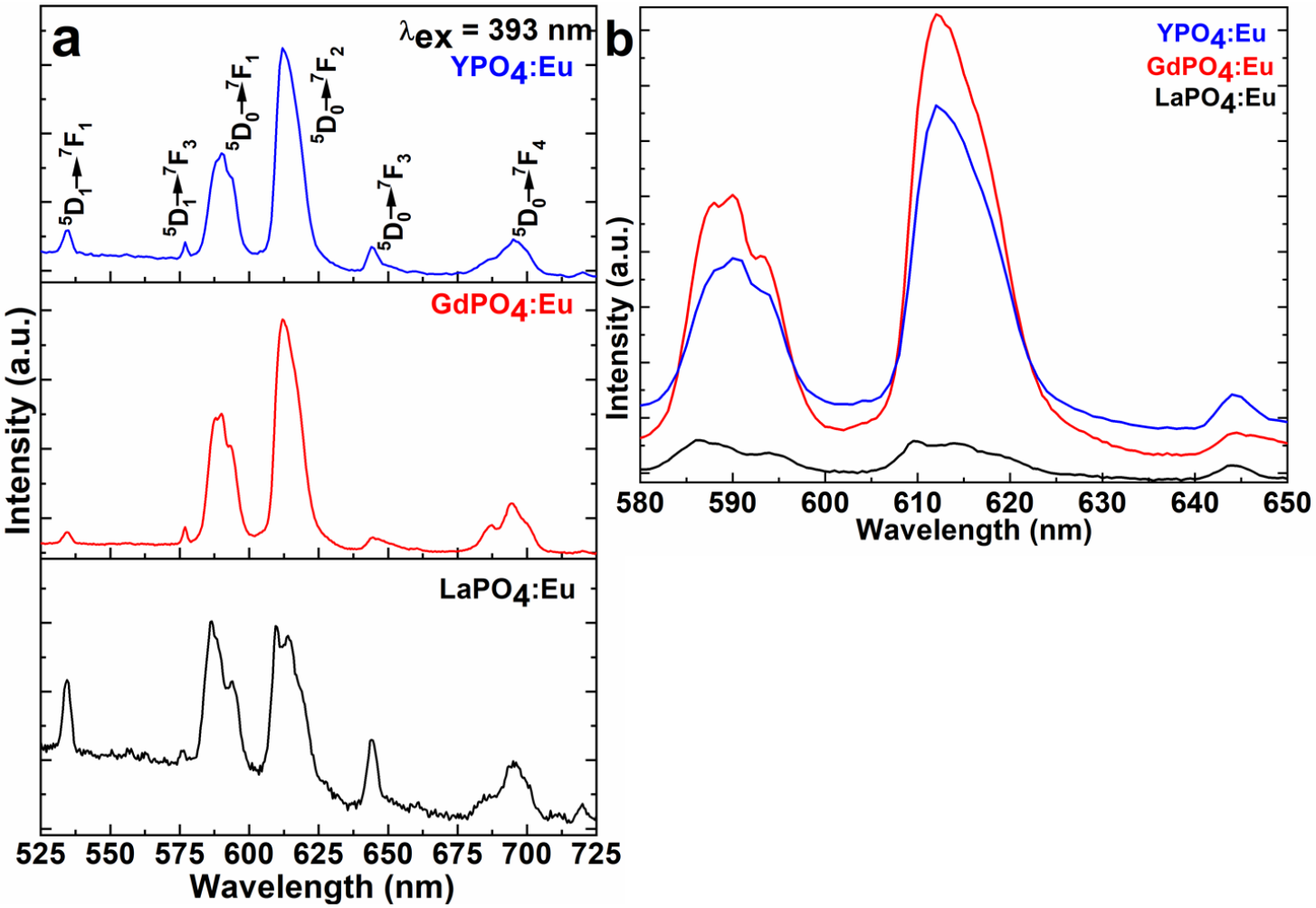
a
λex = 393 nm
YPO4:Eu
5D1→7F1
5D1→7F3
5D0→7F1
5D0→7F2
5D0→7F3
5D0→7F4
GdPO4:Eu
LaPO4:Eu
Intensity (a.u.)
525 550 575 600 625 650 675 700 725
Wavelength (nm)
b
YPO4:Eu
GdPO4:Eu
LaPO4:Eu
Intensity (a.u.)
580 590 600 610 620 630 640 650
Wavelength (nm)

24% Overall Similarity

Top sources found in the following databases:

- 12% Internet database
- Crossref database
- 0% Submitted Works database
- 23% Publications database
- Crossref Posted Content database

TOP SOURCES

The sources with the highest number of matches within the submission. Overlapping sources will not be displayed.

1	Anees A. Ansari, M.A. Majeed Khan. "Eu3+-ion doped LnF3 NPs: Comp... Crossref	6%
2	link.springer.com Internet	3%
3	Anees A. Ansari, M.A. Majeed Khan, Bheeshma P. Singh, Abdul K. Parc... Crossref	2%
4	researchsquare.com Internet	<1%
5	Anees A. Ansari, M.R. Muthumareeswaran, Ruichan Lv. "Coordination c... Crossref	<1%
6	Anees A. Ansari, M. A. Majeed Khan, Sadia Ameen. "Impact of lumines... Crossref	<1%
7	Yanhong Chen, Longhui Sun, Shenzhen Chang, Lijuan Chen, Junwei Zh... Crossref	<1%
8	Anees A. Ansari, M.A Majeed Khan. "Citric acid assisted synthesis of lu... Crossref	<1%

9	scholarscompass.vcu.edu Internet	<1%
10	opus.lib.uts.edu.au Internet	<1%
11	faculty.ksu.edu.sa Internet	<1%
12	iopscience.iop.org Internet	<1%
13	Anees A Ansari, Abdul K. Parchur, Joselito P. Labis, Muhammad Ali Sh... Crossref	<1%
14	Tian, L.. "Variation of the photoluminescence and vacuum ultraviolet e... Crossref	<1%
15	aip.scitation.org Internet	<1%
16	pdfslide.net Internet	<1%
17	mdpi.com Internet	<1%
18	researchgate.net Internet	<1%
19	Anees A. Ansari, Naushad Ahmad, Joselito P. Labis. "Highly colloidal lu... Crossref	<1%
20	Sonia Rodriguez-Liviano, Francisco J. Aparicio, Teresa C. Rojas, Ana B.... Crossref	<1%

21	Anees A. Ansari, M. A. Majeed Khan, Bheeshma P. Singh, Abdul K. Par... Crossref	<1%
22	Laishram Priyobarta Singh, Sri Krishna Srivastava, Ratikant Mishra, Ra... Crossref	<1%
23	José A. Jiménez, Charles L. Crawford. "Optical spectroscopy assessm... Crossref	<1%
24	figshare.com Internet	<1%
25	pubs.rsc.org Internet	<1%
26	coursehero.com Internet	<1%
27	Anees A. Ansari, Shahanavaj Khan, Ali Aldalbahi, Abdul K. Parchur, B. K... Crossref	<1%
28	Francesco Armetta, Vitalii Boiko, Dariusz Hreniak, Cecilia Mortalò, Cris... Crossref	<1%
29	María T. Colomer, Angel L. Ortiz. "Effect of Tb3+ doping and self-gener... Crossref	<1%
30	Santosh K. Gupta, Hisham Abdou, Yuanbing Mao. "Pressure-induced si... Crossref	<1%
31	Shahanavaj Khan, Anees A. Ansari, Christian Rolfo, Andreia Coelho, Ma... Crossref	<1%
32	Shelan M. Mustafa, Azeez A. Barzinjy, Abubaker H. Hamad, Samir M. H... Crossref	<1%

33	Zhongju ZHANG, Jing SHI, Xiaoyan WANG, Sida LIU, Xin WANG. "Vibrat... Crossref	<1%
34	dspace.ncl.res.in:8080 Internet	<1%
35	Anees A. Ansari. "Photochemical studies of monodispersed YPO 4 :Eu ... Crossref	<1%
36	Anees A. Ansari. "Role of surface modification on physicochemical pro... Crossref	<1%
37	Ganngam Phaomei, W. Rameshwor Singh. "Effect of solvent on lumine... Crossref	<1%
38	Niroj Kumar Sahu, R. S. Ningthoujam, D. Bahadur. " Disappearance and ... Crossref	<1%
39	Qiang Wan. "Eu3+-doped LaPO4 and LaAlO3 nanosystems and their lu... Crossref	<1%
40	S. Lange. "Luminescence of ZrO2 and HfO2 thin films implanted with E... Crossref	<1%
41	Santosh K. Gupta, Maya Abdou, Jose P. Zuniga, Alexander A. Puretzky,... Crossref	<1%
42	kareemskpa.weebly.com Internet	<1%
43	library.ncl.res.in Internet	<1%
44	nagaokaut.repo.nii.ac.jp Internet	<1%

45	degruyter.com Internet	<1%
46	hindawi.com Internet	<1%
47	Abdul Kareem Parchur, Amresh Ishawar Prasad, Shyam Bahadur Rai, R... Crossref	<1%
48	Tian, L.. "New red phosphors BaZr(BO"3)"2 and SrAl"2B"2O"7 doped wit... Crossref	<1%
49	Xiaoyan Yang, Ye Zhang, Lin Xu, Zheng Zhai, Mingzhen Li, Meng Li, Xia... Crossref	<1%
50	"Phosphors, Up Conversion Nano Particles, Quantum Dots and Their A... Crossref	<1%
51	Anees A. Ansari, Aslam Khan, Maqsood A. Siddiqui, Naushad Ahmad, ... Crossref	<1%
52	Anees A. Ansari, Joselito P. Labis, M. Aslam Manthrammel. "Designing... Crossref	<1%
53	Ruoxue Yan, Xiaoming Sun, Xun Wang, Qing Peng, Yadong Li. "Crystal ... Crossref	<1%
54	Santosh K. Gupta, Jose P. Zuniga, Partha Sarathi Ghosh, Maya Abdou, ... Crossref	<1%
55	da Costa, Ohanna Maria Menezes Madeiro, and W.M. de Azevedo. "Hig... Crossref	<1%